The five homologous CiaR-controlled Ccn sRNAs of *Streptococcus pneumoniae* modulate Zn-resistance.

Nicholas R. De Lay[1,4#], Nidhi Verma[1], Dhriti Sinha[1], Abigail Garrett[2], Maximillian Osterberg[3], Spencer Reiling[1], Daisy Porter[1], David P. Giedroc[3], and Malcolm E. Winkler[2]

[1]Department of Microbiology and Molecular Genetics, McGovern Medical School, University of Texas Health Science Center, Houston, TX 77030, USA

[2]Department of Biology, Indiana University Bloomington, Bloomington, Indiana 47405

[3]Department of Chemistry, Indiana University, Bloomington, Bloomington, Indiana 47405

[4]MD Anderson Cancer Center UTHealth Graduate School of Biomedical Sciences, University of Texas Health Science Center, Houston, TX 77030, USA

Running Title: Loss of the Ccn sRNAs cause Zn hypersensitivity

Keywords: small RNA; post-transcriptional regulation; Zn homeostasis; Mn homeostasis; CiaRH

Correspondence should be sent to Nicholas R. De Lay (Tel: +1 (713) 500-6293; Email: nicholas.r.delay@uth.tmc.edu)

ABSTRACT

Zinc is a vital transition metal for *Streptococcus pneumoniae*, but is deadly at high concentrations. Zn intoxication of *S. pneumoniae* results from a deficiency in Mn, which is required for key metabolic enzymes and defense against oxidative stress. Here, we report our identification and characterization of the function of the five homologous, CiaRH-regulated Ccn sRNAs in controlling *S. pneumoniae* virulence and metal homeostasis. We show that deletion of all five *ccn* genes (*ccnA*, *ccnB*, *ccnC*, *ccnD*, and *ccnE*) from *S. pneumoniae* strains D39 (serotype 2) and TIGR4 (serotype 4) causes Zn hypersensitivity and an attenuation of virulence in a murine invasive pneumonia model. We provide evidence that addition of Zn disproportionately impairs Mn uptake by the Δ*ccnABCDE* mutants. Consistent with a response to Mn starvation, expression of genes encoding the CzcD Zn exporter and the Mn-independent ribonucleotide reductase, NrdD-NrdG, were increased in the Δ*ccnABCDE* mutant relative to its isogenic *ccn*$^+$ parent strain. The growth inhibition by Zn that occurs as the result of loss of the *ccn* genes is rescued by supplementation with Mn or Oxyrase™, a reagent that removes dissolved oxygen. Lastly, we found that the Zn-dependent growth inhibition of the Δ*ccnABCDE* strain was not altered by deletion of *sodA*, whereas the *ccn*$^+$ Δ*sodA* strain phenocopied the Δ*ccnABCDE* strain. Overall, our results indicate that the Ccn sRNAs have a crucial role in preventing oxidative stress in *S. pneumoniae* during exposure to excess Zn by modulating Mn uptake.

AUTHOR SUMMARY

Zn and Mn are essential micronutrients for many bacteria, including *Streptococcus pneumoniae*. While Zn performs vital structural or catalytic roles in certain proteins, in excess, Zn can inhibit Mn uptake by *S. pneumoniae* and displace, but not functionally replace Mn from key enzymes including superoxide dismutase A (SodA). Here, we show that the Ccn small regulatory RNAs

promote *S. pneumoniae* Mn uptake and resistance to the oxidative stress. Furthermore, we demonstrate that these small regulatory RNAs modulate the ability of *S. pneumoniae* to cause invasive pneumonia. Altogether, these findings reveal a new layer of regulation of *S. pneumoniae* Zn and Mn homeostasis and suggest that there are factors in addition to known transporters that modulate intracellular Mn levels.

INTRODUCTION

Small regulatory RNAs have been established as fundamental regulators of gene expression in bacteria and are involved in controlling nearly every aspect of bacterial physiology, metabolism, and behavior (*1*-*3*). Two basic classes of small regulatory RNAs have been identified and characterized, those that control gene expression by directly interacting with transcripts via hydrogen bonding between complementary or wobble base-pairs and others that indirectly effect transcript abundance by titrating an RNA or DNA-binding protein (*4, 5*). Interactions between the former class of riboregulators, henceforth referred to as sRNAs, and their cognate target transcripts can result in changes in their transcription, translation, and/or stability depending on many factors include the sequence, accessibility, structure, and location of the sRNA binding site. One of the most facile modes of regulation discovered involves the sRNA binding within or adjacent to the translation initiation region blocking the 16S rRNA within the 30S ribosomal subunit from base-pairing with the complementary Shine-Delgarno sequence, or ribosome binding site, within the mRNA. Many other elegant mechanisms of sRNA-based gene regulation have been uncovered (*6*-*8*). While a large amount of progress has been made towards understanding the contribution of sRNAs to the response of Gram-negative bacteria such as *Escherichia coli* to internally and externally derived stresses, environmental cues, and host interactions, much less headway has been achieved in understanding the functions of sRNAs in Gram-positive bacteria, particularly, *Streptococcus pneumoniae*.

The Gram-positive, ovoid diplococcus *S. pneumoniae* is a leading cause of lower respiratory infection morbidity and mortality worldwide resulting in nearly 2 million deaths per year (*9*). We and others have discovered 100s of putative sRNAs in *S. pneumoniae* (*10-15*), but the functions of almost all of them remains a mystery. Among the first sRNAs identified in *S. pneumoniae* were the five homologous Ccn sRNAs (CcnA, CcnB, CcnC, CcnD, and CcnE), which were shown to be transcribed in response to activation of the CiaRH two-component system (*15, 16*); expression of the CiaRH two-component systems is induced by penicillin and sialic acid (*17, 18*). Shortly after the discovery of the five Ccn sRNAs, Tsui, Mukerjee (Sinha), et al demonstrated that CcnA negatively regulates competence and the *comCDE* mRNA encoding the precursor of the competence stimulating peptide and the two-component system that responds to this signal and activates competence (*15*). Schnorpfeil et al then formally demonstrated that the five Ccn sRNAs negatively regulate competence by base-pairing with the *comCDE* mRNA (*19*). Other likely targets post-transcriptionally regulated by the Ccn sRNAs were identified in that study including mRNAs encoding components of a galactose transporter (*spd_0090*), a formate-nitrate transporter (*nirC*), branched-chain amino acid transporter (*brnQ*) and a toxin *(shetA*), but direct regulation of these targets by the Ccn sRNAs has not yet been shown (*19*). One of these five homologous sRNAs, CcnE, has also been implicated in *S. pneumoniae* virulence in a murine invasive pneumonia model (*12*).

Here, we report our discovery of a role for the five Ccn sRNAs in controlling *S. pneumoniae* virulence and Zn resistance. Specifically, we show that deletion of the genes encoding the five Ccn sRNAs attenuates the virulence of *S. pneumoniae* strains D39 and TIGR4 in a murine invasive pneumonia model. Additionally, we show that loss of the Ccn sRNAs leads *S. pneumoniae* D39 and TIGR4 to become hypersensitive to Zn toxicity. Altogether, our results indicate that the Ccn sRNAs promote Mn uptake leading into increased Zn resistance due to an increase in the amount of active superoxide dismutase A (SodA).

RESULTS

The Ccn sRNAs are important for *S. pneumoniae* pathogenesis. Work from a prior study (*12*) indicated that deletion of one of the five Ccn sRNA genes (*ccnE*) reduced *S. pneumoniae* serotype 4 strain TIGR4 virulence in a murine invasive pneumoniae model. In that study, the authors also discovered by Tn-seq that transposon insertions in *ccnE* reduced *S. pneumoniae* strain TIGR4 fitness in murine lungs, whereas transposon insertions in *ccnA* had no significant impact on its fitness in the murine lung, nasopharynx, or blood. To determine the contribution of the Ccn sRNAs to the virulence of the *S. pneumoniae* serotype 2 strain D39 in a murine invasive pneumonia model, we initially made single deletions of *ccnA*, *ccnB*, *ccnC, ccnD*, or *ccnE* and a quintuple deletion of all five *ccn* genes in a strain background harboring the *rpsL1* allele (IU1781). Next, we evaluated the growth of these strains in BHI broth at 37^{o}C in an atmosphere of 5% CO_2. Neither deletion of any single Ccn sRNA gene or all five of them had any significant effect on growth rate, although the growth yield of the Δ*ccnE* strain was slightly reduced (Figs. 1A, S1A, and S1C). We then determined the consequence of these deletions on *S. pneumoniae* pathogenicity in a murine invasive pneumonia model (see Materials and Methods). While removal of any single *ccn* gene had no significant impact on its virulence in mice (Fig. S2), deletion of all five *ccn* genes attenuated *S. pneumoniae* strain D39 pathogenicity increasing median survival time from 43 h to 67 h (Fig. 2A).

To confirm that the *ccn* genes are generally important for *S. pneumoniae* virulence and is not an attribute specific to strain D39, we also deleted all five *ccn* genes from a serotype 4 TIGR4 strain harboring the *rpsL1* allele (NRD10220) and measured the impact of these deletions on its growth and virulence using the same murine invasive pneumonia model. As shown in Fig. 1D, deletion of all five *ccn* genes did have an effect on growth rate of *S. pneumoniae* TIGR4 in BHI broth incubated at 37^{o}C with an atmosphere of 5% CO_2. To validate the effect of the *ccnABCDE* deletion on *S. pneumoniae* TIGR4 growth, we reconstructed the quintuplet deletion strain from scratch, but this time we subsequently replaced the mutant *rpsL* allele conferring streptomycin

resistance that aided in construction of the unmarked deletions of the *ccn* genes back to the wild type *rpsL* allele. Next, we tested the growth of that strain and its parental *ccn*$^+$ TIGR4 strain in BHI broth at 37^{o}C under an atmosphere of 5% CO_2. Again, we saw a substantial reduction in growth rate when all five *ccn* genes were deleted (Fig. S3A). The *ccnABCDE* deletion also resulted in a marked attenuation of *S. pneumoniae* TIGR4 virulence increasing the survival rate of ICR outbred mice from 0% to 50% (Fig. 2B). Two of the mice that survived infection with the TIGR4 Δ*ccnABCDE* strain had no detectable bacteria in the blood and the other two mice had 1000 and 2750 CFUs per mL of blood, respectively, which was far below 10^7 bacteria found in moribund mice that were infected with the *ccn*$^+$ parent strain. Our results show that the *ccn* genes are important for *S. pneumoniae* pathogenesis.

The Ccn sRNAs impact expression of Zn and Mn-related genes. To discover a basis for the defect in *S. pneumoniae* virulence caused by the deletion of the five *ccn* genes, we compared global gene expression by high throughput RNA-sequencing (RNA-seq) between *S. pneumoniae* strain D39 or TIGR4 and the derived Δ*ccnABCDE* mutant strains grown to exponential phase (OD_{620} between 0.15 and 0.2) in BHI broth at 37^{o}C in an atmosphere of 5% CO_2. In the *S. pneumoniae* D39 strain background, the *ccnABCDE* deletion resulted in down-regulation of 3 genes and up-regulation of 113 genes by 2-fold or more ($P_{adj} < 0.05$) (Table S3). In contrast, deletion of the *ccn* genes from the TIGR4 strain resulted in down-regulation of 25 genes and up-regulation of 97 genes by 2-fold or greater ($P_{adj} < 0.05$) (Table S4). 37 genes were up-regulated by 2-fold ($P_{adj}<0.05$) in the *ccnABCDE* deletion strain in both the D39 and TIGR4 backgrounds (Table 1); among these differentially expressed genes were iron uptake system genes (*piuB*, *piuC*, *piuD*, and *piuA*), a Zn-responsive ECF (energy-coupling factor) transport gene SPD_1267/SP_1438, and *czcD* encoding a Zn/Cd exporter that provides Zn and Cd resistance. To validate our RNA-seq data, we first measured abundance of *piuB*, *spd_1267*, and *czcD*

transcripts in RNA samples isolated for the RNA-seq experiment from *S. pneumoniae* strain D39 and derived Δ*ccnABCDE* strain by reverse transcriptase droplet digital PCR (RT-ddPCR). Consistent with our RNA-seq data the *piuB, spd_1267,* and *czcD* transcripts were up-regulated by 3.47, 10.5, and 1.93-fold respectively in the Δ*ccnABCDE* strain compared to its parental D39 strain grown in BHI broth (Fig. 3A, B, and C). Using RT-ddPCR analysis of the RNA samples isolated from exponential cultures of *S. pneumoniae* TIGR4 and derived Δ*ccnABCDE* mutant strain grown in BHI broth at 37°C under an atmosphere of 5% CO_2, we also observed a 2.45 increase in the abundance of the *czcD* mRNA in the *ccn* mutant as compared to its parental strain (Fig. 3E). Altogether, these data suggested to us that removal of the *ccn* genes from *S. pneumoniae* was leading to an increase in the intracellular abundance of Zn relative to Mn, and to cope with this stress, the *ccn* mutant strain was increasing expression of the CzcD Zn exporter.

Table 1: Genes significantly, differentially expressed between a Δ*ccnABCDE* and *ccn*⁺ strain in both the *S. pneumoniae* D39 and TIGR4 background during exponential growth in BHI broth[a]

D39 locus tag	Gene	Known or predicted function	D39 fold change	TIGR4 fold change
SPD_0025		tRNA-specific adenosine-34 deaminase	84.3	144
SPD_0027	*dut*	deoxyuridine 5'-triphosphate nucleotidohydrolase	3.52	4.39
SPD_0028		hypothetical protein	3.80	3.40
SPD_0029	*radA*	DNA repair protein	3.55	2.80
SPD_0090		galactose ABC transport protein	2.09	2.00
SPD_0104		aggregation-promoting factor	2.69	2.27
SPD_0222	*gpmB1*	phosphoglycerate mutase family protein	25.0	22.9
SPD_0243	*uppS*	undecaprenyl diphosphate synthase	5.97	4.42
SPD_0244	*cdsA*	phosphatidate cytidylyltransferase	5.50	4.49
SPD_0245	*eep*	intramembrane protease	5.57	4.19
SPD_0246	*proS*	prolyl-tRNA synthetase	5.91	4.68
SPD_0247	*bglA*	6-phospho-β-glucosidase	3.57	3.35
SPD_0308	*clpL*	ATP-dependent protease subunit	13.7	2.71
SPD_0460	*dnaK*	protein chaperone	3.97	2.01
SPD_0501	*licT*	β-glucoside operon antiterminator	2.91	4.77
SPD_0502	*bglF*	β-glucoside PTS transporter subunit	3.07	5.65

SPD_0503	*bglA-2*	6-phospho- β-glucosidase	2.57	4.79
SPD_0615	*glnH3*	degenerate glutamine ABC transporter subunit	11.6	4.05
SPD_0616	*glnQ3*	glutamine ABC transporter subunit	8.90	3.07
SPD_0617	*glnP3b*	glutamine ABC transporter subunit	11.1	3.63
SPD_0618	*glnP3a*	glutamine ABC transporter subunit	11.8	2.98
SPD_0775		acetyltransferase	3.29	2.71
SPD_1045		degenerate DUF3884 domain protein	4.73	3.16
SPD_1046	*lacG-2*	6-phospho-β-galactosidase	3.56	2.92
SPD_1267		ECF transporter subunit	11.1	2.14
SPD_1638	*czcD*	Cd/Zn exporter	2.69	2.66
SPD_1649	*piuB*	Fe uptake transporter subunit	5.13	2.43
SPD_1650	*piuC*	Fe uptake transporter subunit	4.45	2.01
SPD_1651	*piuD*	Fe uptake transporter subunit	4.22	2.15
SPD_1652	*piuA*	Fe uptake transporter subunit	4.38	2.25
SPD_1748	*pneA2*	lantibiotic peptide	2.19	2.16
SPD_1749	*lanM*	lanthionine biosynthesis protein	2.49	2.29
SPD_1750	*wrbA*	FAD-dependent flavoprotein	3.00	2.69
SPD_1751		hypothetical protein	2.56	3.16
SPD_1752	*clyB*	toxin secretion ABC transporter	3.58	3.22
SPD_1753		epidermin leader peptide processing serine protease	2.44	2.87
SPD_1932	*malP*	malodextrin phosphorylase	2.58	2.58

[a]RNA extraction and mRNA-seq analyses were performed as described in *Materials and Methods*. RNA was prepared from cultures of strains IU1781 (D39 *rpsL1*), NRD10176 (D39 *rpsL1* Δ*ccnABCDE*), NRD10220 (TIGR4 *rpsL1*), and NRD10266 (TIGR4 *rpsL1* Δ*ccnABCDE*) (Table S1 and S2). Fold changes (2.0-fold cut-off) and adjusted P-values (Pval <0.05) are based on three independent biological replicates.

Absence of the *ccn* genes causes S. *pneumoniae* to become hypersensitive to Zn. If the absence of the *ccn* genes from *S. pneumoniae* leads to an imbalance of transition metals with higher levels of Zn relative to Mn, then we would expect that increasing the concentration of Zn present in the medium would disproportionately impair the growth of the Δ*ccnABCDE* mutant relative to the isogenic *ccn*$^+$ strain. Previous studies have indicated that Becton-Dickinson (BD) BHI broth typically contains ~20 μM Zn and 200 nM Mn (*20, 21*). We first compared growth of

strain D39 and derived Δ*ccnA*, Δ*ccnB*, Δ*ccnC*, Δ*ccnD*, Δ*ccnE*, and Δ*ccnABCDE* strains in BHI broth alone or supplemented with 0.2 mM Zn at 37°C under an atmosphere of 5% CO_2. No significant difference was observed in growth rate between strain D39 and derived Δ*ccnA*, Δ*ccnB*, Δ*ccnC*, and Δ*ccnD* mutant strains in BHI in the presence or absence of 0.2 mM added Zn (Fig. S1), although the growth yield for the *ccnE* mutant was lower in BHI in the presence and absence of Zn. As noted above, growth the strain D39 and derived Δ*ccnABCDE* mutant strain was similar in BHI broth alone (Fig. 1A.) In contrast, the absence of all five *ccn* genes led to an obvious impairment in growth rate in BHI supplemented with 0.2 mM Zn (Fig. 1B) This growth deficiency relative to the *ccn*$^+$ parental strain was also observed for the Δ*ccnABCDE* strain when Zn was increased in BHI broth to 0.4 mM (Fig. 1C). Consistently, addition of Zn at 0.4 mM severely reduced the growth rate of the *ccn*$^+$ D39 strain. Reintroduction of *ccnC* and *ccnD* expressed from their native promoters at ectopic loci partially ameliorated the growth defect of the Δ*ccnABCDE* mutant strain in BHI supplemented with 0.2 mM or 0.4 mM Zn, whereas insertion of copies of *ccnA, ccnB*, and *ccnD* with their native promoter at the *bgaA* and CEP loci completely corrected the growth deficiency of this quintuple *ccn* mutant (Figs. 1B and 1C) under these growth conditions. To verify that the Zn hypersensitivity caused by the deletion of all five *ccn* genes was not specific to the serotype 2 strain D39, we also tested the effect of the quintuple *ccn* deletion on the growth of the serotype 4 TIGR4 strain in BHI broth supplemented with Zn. Consistent with our results observed for strain D39, deletion of the Ccn sRNA genes from TIGR4 led to a growth impairment in BHI when Zn was added at a final concentration of 0.2 or 0.4 mM (Figs. 1D-F and S3). Curiously, Zn at the highest concentration used had less of an effect on TIGR4 growth than it did on the D39 strain. Overall, these results indicate that Ccn sRNAs promote *S. pneumoniae* Zn tolerance.

The Zn-hypersensitivity that occurs in the absence of the Ccn sRNA genes is due to a reduction in cellular Mn levels. *S. pneumoniae* is a Mn-centric bacteria encoding several Mn-requiring enzymes including superoxide dismutase (SodA), a capsule regulatory kinase (CpsB), phosphoglucomutase (Pgm), phosphopentomutase (DeoB), a cell division regulating phosphatase (PhpP), an aerobic ribonucleotide reductase (NrdEF), pyruvate kinase (PyK), and lactate dehydrogenase (Ldh). Mis-metalation of these Mn-dependent enzymes by Zn, which inhibits their enzymatic activity (*22, 23*), can occur when the internal ratio of Zn-to-Mn is high. Additionally, the substrate binding component of the PsaBCA Mn ATP binding cassette (ABC) type transporter, the only known Mn importer in *S. pneumoniae*, has been shown to bind Zn tightly, blocking Mn uptake (*20, 24*). Our RNA-seq and RT-ddPCR data above indicated that expression of the CzcD Zinc exporter, which is expressed in response to high levels of Zn relative to Mn (*25, 26*), is up-regulated in *S. pneumoniae* strains lacking the *ccn* genes (Fig. 3C and E). Based on these results and the published data mentioned above, we hypothesized that Zn-hypersensitivity caused by the removal of all five *ccn* genes from the *S. pneumoniae* genome is due to reduced Mn uptake. If this postulate is correct, then the Zn-dependent growth inhibition that occurs when the *S. pneumoniae* Δ*ccnABCDE* mutant strain is grown in BHI broth supplemented with 0.2 mM Zn should be rescued by inclusion of an equimolar amount of Mn into the medium. As shown in Fig. 4, the growth impairment of the Δ*ccnABCDE* mutant of *S. pneumoniae* D39 or TIGR4 strain in BHI broth with 0.2 mM Zn is cured by addition of 0.2 mM Mn consistent with our model.

To directly test whether or not the levels of transition metals are perturbed in strains lacking the *ccn* genes, we measured total cell associated transition metals in *S. pneumoniae* strain D39, derived Δ*ccnABCDE* mutant, and the Δ*ccnABCDE* strain complemented with *ccnA*, *ccnB*, and *ccnD* by inductively coupled plasma-mass spectrometry (ICP-MS). During exponential growth (OD_{620} of ~0.2) in BHI broth alone or supplemented with 0.2 mM Zn, there was no significant difference in Zn abundance among these strains (Fig 5A). Similarly, Mn levels were comparable

among all tested strains when grown to exponential phase in BHI broth alone (Fig. 5B). However, there was a modest, but statistically significant (P = 0.039), 22% reduction in total cell associated Mn in the Δ*ccnABCDE* mutant compared to its parental *ccn*$^+$ strain, which was partially complemented by *ccnA*, *ccnB*, and *ccnD*. Thus, our evidence that Mn supplementation eliminated the growth deficiency of the *ccn*$^-$ strain caused by excess Zn and that the amount of Mn associated with this mutant strain was reduced compared to the *ccn*$^+$ strain when exposed to a high Zn concentration suggest that the Ccn sRNAs are important for preserving Mn homeostasis, when *S. pneumoniae* encounters a Zn-rich environment.

Oxidative stress due to reduced levels of active superoxide dismutase A contributes to the Zn hypersensitivity of the *S. pneumoniae* strain lacking the Ccn sRNAs. To discover the molecular basis for the Zn hypersensitivity caused by loss of the *ccn* genes, we turned to an RNA-seq based approach. Briefly, we compared transcript abundance in RNA isolated from *S. pneumoniae* strain D39 and derived Δ*ccnABCDE* strain grown to exponential phase (OD_{620} of ~0.2) at 37^{o}C under an atmosphere of 5% CO_2 in BHI broth supplemented with 0.2 mM Zn. Similar to our RNA-seq performed with these strains in the absence of Zn supplementation, we observed a 2.33-fold increase in expression of the CzcD Zn exporter specifying mRNA and a 9.5-fold increase in the Spd_1267 Zn-responsive ECF-type transporter producing mRNA in the Δ*ccnABCDE* mutant compared to its *ccn*$^+$ parent strain (Tables 2 and S5). Interestingly, we also saw a 1.90-fold decrease (P_{adj} = $1.81x10^{-43}$) in expression of the *sodA* mRNA, encoding superoxide dismutase A, in the Δ*ccnABCDE* mutant strain, which was just below our arbitrary two-fold cutoff (Table S5). We subsequently measured the relative abundance of these transcripts by RT-ddPCR and northern blot analysis (Figs. 3B, C, and D) and were able to confirm our RNA-seq results indicating up-regulation of *spd_1267* and *czcD* mRNAs and down-regulation of the *sodA* mRNA abundance when the *ccn* genes were deleted from *S. pneumoniae*. This result was

intriguing to us since a prior study found that Mn starvation of *S. pneumoniae* cells due to exposure to high concentrations of Zn relative to Mn led to a reduction in the transcription of *sodA* and a reduction in superoxide dismutase activity (*22*). Furthermore, Eijkelkamp *et* al discovered that deletion of *sodA* had no significant impact on *S. pneumoniae* growth under Mn replete conditions, but was vital for growth in media containing a high Zn-to-Mn ratio (*22*).

Table 2: Genes significantly, differentially expressed between a *S. pneumoniae* D39 and derived Δ*ccnABCDE* strain in both BHI alone or supplemented with Zn[a]

D39 locus tag	Gene	Known or predicted function	Fold change (BHI)	Fold change (BHI+Zn)
SPD_0025		tRNA-specific adenosine-34 deaminase	84.3	49.0
SPD_0027	*dut*	deoxyuridine 5'-triphosphate nucleotidohydrolase	3.52	3.76
SPD_0028		hypothetical protein	3.80	3.02
SPD_0029	*radA*	DNA repair protein	3.55	2.95
SPD_0080	*pavB*	cell wall surface anchor family protein	6.69	6.32
SPD_0163		DNA binding protein	2.00	2.07
SPD_0222	*gpmB1*	phosphoglycerate mutase family protein	25.0	21.7
SPD_0243	*uppS*	undecaprenyl diphosphate synthase	5.97	7.61
SPD_0244	*cdsA*	phosphatidate cytidylyltransferase	5.50	7.77
SPD_0245	*eep*	intramembrane protease	5.57	8.59
SPD_0246	*proS*	prolyl-tRNA synthetase	5.91	9.65
SPD_0247	*bglA*	6-phospho-β-glucosidase	3.57	4.73
SPD_0277	*bglA-1*	6-phospho-β-glucosidase	3.53	2.73
SPD_0279	*celB*	cellobiose PTS transporter subunit	5.05	2.97
SPD_0308	*clpL*	ATP-dependent protease subunit	13.7	9.55
SPD_0350	*vraT*	cell wall-active antibiotic response protein	2.19	2.62
SPD_0351	*vraS*	two-component system histidine kinase	2.29	2.74
SPD_0352	*vraR*	two-component system response regulator	2.31	2.70
SPD_0353	*alkD*	degenerate DNA alkylation repair enzyme	2.11	2.67
SPD_0354	*alkD*	degenerate DNA alkylation repair enzyme	2.37	2.69
SPD_0458	*hrcA*	heat inducible transcription repressor	3.62	3.69
SPD_0459	*grpE*	heat shock protein	3.77	3.87
SPD_0460	*dnaK*	protein chaperone	3.97	3.82
SPD_0461	*dnaJ*	protein chaperone	3.50	3.52
SPD_0474	*blpZ*	immunity protein	2.40	2.05
SPD_0501	*licT*	β-glucoside operon antiterminator	2.91	5.26
SPD_0502	*bglF*	β-glucoside PTS transporter subunit	3.07	4.65
SPD_0503	*bglA-2*	6-phospho- β-glucosidase	2.57	3.75
SPD_0537		putative Zn-dependent protease	2.07	2.21

SPD_0615	*glnH3*	degenerate glutamine ABC transporter subunit	11.6	18.0
SPD_0616	*glnQ3*	glutamine ABC transporter subunit	8.90	16.8
SPD_0617	*glnP3b*	glutamine ABC transporter subunit	11.1	15.8
SPD_0618	*glnP3a*	glutamine ABC transporter subunit	11.8	15.1
SPD_0681		hypothetical protein	2.82	5.45
SPD_0701	*ciaR*	two-component response regulator	2.72	2.56
SPD_0702	*ciaH*	two-component histidine kinase	2.80	3.01
SPD_0775		acetyltransferase	3.29	3.61
SPD_0803		putative phage shock protein C		
SPD_0804		ABC transporter ATP-binding protein	2.28	3.01
SPD_0805		ABC transporter permease protein	2.43	3.15
SPD_0913		extracellular protein	3.39	3.31
SPD_0938		degenerate TN5252 relaxase	9.35	5.06
SPD_0940	*rrfD*	UDP-N-acetyl-D-mannosaminouronic acid dehydrogenase.	3.95	5.31
SPD_0942		hypothetical protein	2.25	2.41
SPD_0943		hypothetical proein	2.41	2.43
SPD_0944		nodulation protein L	2.24	2.38
SPD_0946		hypothetical protein	2.16	3.27
SPD_0947		hypothetical protein	2.69	3.97
SPD_0948	*nikS*	nikkomycin biosynthesis protein	3.73	4.29
SPD_0949		N-acetylneuraminate synthase	2.38	4.85
SPD_0950	*mefE*	macrolide ABCE transporter subunit	2.44	3.99
SPD_1045		degenerate DUF3884 domain protein	4.73	6.81
SPD_1046	*lacG-2*	6-phospho-b-galactosidase	3.56	7.28
SPD_1047	*lacE-2*	lactose PTS transporter subunit	4.21	6.33
SPD_1049	*lacT*	β-glucoside *bgl* operon antiterminator	3.23	3.48
SPD_1114		hypothetical protein	13.5	5.37
SPD_1267		ECF transporter subunit	11.1	9.53
SPD_1297	*pdxS*	pyridoxal 5'-phosphate synthase	2.02	2.04
SPD_1506	*axe1*	acetyl xylan esterase 1	3.62	2.68
SPD_1615		degenerate hypothetical protein	4.02	2.09
SPD_1638	*czcD*	Cd/Zn exporter	2.69	2.33
SPD_1709	*groL*	HSP60 family chaperone	2.58	2.38
SPD_1710	*groES*	HSP60 family chaperone	2.25	2.31
SPD_1716		hypothetical protein	2.56	5.62
SPD_1717		membrane protein	2.40	5.22
SPD_1718		LytR/AlgR family response regulator	2.44	4.58
SPD_1746		hypothetical protein	2.96	4.25
SPD_1747	*pneA1*	lantibiotic peptide	2.02	4.29
SPD_1748	*pneA2*	lantibiotic peptide	2.19	4.60
SPD_1749	*lanM*	lanthionine biosynthesis protein	2.49	2.37
SPD_1750	*wrbA*	FAD-dependent flavoprotein	3.00	2.85
SPD_1751		hypothetical protein	2.56	4.07
SPD_1752	*clyB*	toxin secretion ABC transporter	3.58	4.02
SPD_1753		epidermin leader peptide processing serine protease	2.44	3.00
SPD_1769		membrane protein	2.29	3.42

SPD_1932	*malP*	malodextrin phosphorylase	2.58	2.95
SPD_1933	*malQ*	4-α-glucanotransferase	2.76	2.77
SPD_1990		mannose PTS transporter subunit	2.01	13.8
SPD_1994	*fucA*	L-fuculose phosphate aldolase	2.35	8.69
SPD_2034	*comFC*	phosphororibosyltransferase domain protein	32.7	14.1
SPD_2035	*comFA*	DNA transporter ATPase	8.88	10.2
SPD_2068	*htrA*	serine protease	2.79	2.13
SPD_2069	*parB*	chromosome partitioning protein	3.04	2.88

[a]RNA extraction and mRNA-seq analyses were performed as described in *Materials and Methods*. RNA was prepared from cultures of strains IU1781 (D39 *rpsL1*) and NRD10176 (D39 *rpsL1* Δ*ccnABCDE*) grown to exponential phase in BHI alone or supplemented with 0.2 mM $ZnSO_4$ (Table S1 and S2). Fold changes (2.0-fold cut-off) and adjusted P-values (Pval <0.05) are based on three independent biological replicates.

To initially examine whether the growth deficiency of the Δ*ccnABCDE* mutant relative to the *ccn*$^+$ D39 strain was due in part to oxidative stress, we evaluated the impact of addition of Oxyrase™, an enzyme mixture that removes molecular oxygen by reducing it to water, on the growth of these strains in BHI broth alone or supplemented with 0.2 mM or 0.4 mM Zn (Fig 6A, B, and C) under an atmosphere of 5% CO_2. Once again, we observed that deletion of *ccnA*, *ccnB*, *ccnC*, *ccnD*, and *ccnE* from *S. pneumoniae* strain D39 had no significant impact on growth in BHI alone. However, under these growth conditions, the addition of Oxyrase™ reduced the growth rate of both the *ccn*$^+$ and ccn$^-$ strains to a similar extent (Fig. 6A). As we anticipated, addition of Oxyrase™ to BHI supplemented with Zn (0.2 mM) improved the growth rate of the Δ*ccnABCDE* strain to that observed for the *ccn*$^+$ D39 parent strain (Fig. 6B). Interestingly, addition of Oxyrase™ improved the growth rate of both strains in BHI with 0.4 mM Zn and eliminated any growth differences between them (Fig. 6C). Finally, we examined the contribution of *sodA* to the growth of *S. pneumoniae* D39 and derived Δ*ccnABCDE* mutant strain. In BHI broth alone or supplemented with 0.2 mM Zn, deletion of *sodA* reduced the growth rate of the *ccn*$^+$ strain, but

had no significant reduction in growth rate of the Δ*ccnABCDE* mutant strain (Fig. 7). Based on these results, we concluded that the amount of functional SodA was negligible in the *S. pneumoniae* strain lacking the Ccn sRNAs and thus, deleting *sodA* did not significantly impact its growth, whereas this deletion does substantially impair growth of the isogenic *ccn*$^{+}$ strain.

DISCUSSION

High density Tn-seq experiments performed more than a decade ago revealed that sRNAs play a crucial role in regulating *S. pneumoniae* virulence including its ability to colonize the blood, nasopharynx, and lungs of its host (*12*). While this discovery in itself may not be surprising, it is astonishing that very little progress has been made towards understanding the functions of these sRNAs given their importance in governing *S. pneumoniae* pathogenesis. Here, we investigated the contribution of the five homologous Ccn sRNAs to *S. pneumoniae* pathogenesis and gene regulation. Not only have we confirmed their crucial role in pneumococcal disease progression (Fig. 2), but also discovered their extensive functions in regulating gene expression and Zn resistance. Specifically, we found that exposure to relatively high, yet host-relevant, Zn concentrations (0.2 mM) disproportionally inhibited growth (Fig 1, 4, 6, and 7) and modestly reduced total cell associated Mn levels (Fig. 5) of *S. pneumoniae* strains lacking genes for the five Ccn sRNAs. This Zn-dependent growth inhibition caused the *ccnABCDE* deletion was completely alleviated by addition of Mn (Fig. 4) or Oxyrase™ (Fig. 6), which removes molecular oxygen by reducing it to water. Furthermore, deletion of *sodA*, encoding the Mn-dependent superoxide dismutase A, from *S. pneumoniae* resulted in a Zn-dependent growth inhibition indistinguishable from that observed for the Δ*ccnABCDE* strain; however, the same deletion had no impact on the growth of the Δ*ccnABCDE* strain (Fig. 7). Altogether, these results indicate that the Ccn sRNAs promote Mn uptake and availability resulting in an increased abundance of active

SodA, which improves the growth of *S. pneumoniae* in a Zn-rich environment due to greater protection from damaging reactive oxygen species.

How do the Ccn sRNAs promote an increased concentration of free intracellular Mn^{2+} cations? Potential mechanisms through which the Ccn sRNAs could increase the concentration of available Mn inside *S. pneumoniae* cells include that the Ccn sRNAs (1) negatively regulate expression of a Mn exporter, (2) positively regulate expression of a Mn importer, (3) reduce production of an intracellular protein or other factor that effectively chelates Mn, or (4) decrease synthesis of a cellular component that would otherwise restrict access of Mn to the periplasmic Mn binding component of the Mn importer. The main Mn exporter of *S. pneumoniae* is MntE (Fig. 8), as deletion of the encoding gene leads to accumulation of total cell associated Mn (*21, 27*). MgtA, designated as a Ca efflux protein, appears to also export Mn, but has a very limited role in this process (Fig. 8) (*28*). Neither MntE or MgtA were up-regulated in either *S. pneumoniae* strain D39 or TIGR4 when the *ccn* genes were deleted (Tables S3 S4, and S5) making it unlikely that the Ccn sRNAs increase intracellular Mn levels by down-regulating expression of these Mn exporter genes. Additionally, we were unable to identify strong Ccn sRNA binding sites in the translation initiation region of *mntE* or *mgtA*, which suggests that these sRNAs do not regulate translation of these transcripts. Finally, if the Ccn sRNAs increase total cell-associated Mn levels by down-regulating MntE expression, then we would expect that deletion of *mntE* would suppress the Zn hypersensitivity of the *S. pneumoniae* Δ*ccnABCDE* mutant; however, this did not occur (Fig S4A and C).

An alternative possibility is that the Ccn sRNAs promote Mn uptake by positively regulating expression of the *psaBCA* operon encoding the only known Mn importer in *S. pneumoniae* (Fig. 8)(*29, 30*). Localized to the inner membrane, PsaB is the ATP binding component whereas PsaC is the permease of this ABC-type transporter. PsaA, the substrate binding component, is located in the periplasm, where it binds Mn. Once again, in our RNA-seq experiments, we did not observe a decrease in expression of the *psaBCA* operon when the *ccn* genes were deleted from *S.*

335 *pneumoniae* strain D39 or TIGR4 (Tables S3, S4, and S5) indicating that the Ccn sRNAs do not
336 positively regulate expression of this Mn importer. Furthermore, if this was the case, then we
337 would expect that deletion of *psaR* encoding the repressor of the *psaBCA* operon (*31, 32*) might
338 suppress the Zn-dependent growth inhibition of the *S. pneumoniae* Δ*ccnABCDE* mutant;
339 however, we did not observe this (Fig. S4B and D).

340 While it remains possible that the Ccn sRNAs regulate production of a factor that chelates
341 intracellular Mn, we did not observe the up-regulation of any *known* Mn-binding proteins via RNA-
342 seq. A final possibility that we surmised could be occurring is that the Ccn sRNAs negatively
343 impact the production or architecture of a structure that could restrict Mn uptake by limiting the
344 diffusion of Mn into the periplasm, where it could be transported by the PsaBCA Mn importer into
345 the cytoplasm. For example, a physical structure that might serve as a permeability barrier to Mn
346 is the polysaccharide capsule that surrounds *S. pneumoniae* diplococci. To test this possibility,
347 we evaluated the impact of deleting the capsule biosynthetic genes on the Zn hypersensitivity of
348 the *S. pneumoniae* Δ*ccnABCDE* mutant. Interestingly, we observed that the *cps2ABCDETFGH*
349 deletion completely suppressed the Zn hypersensitivity of an *S. pneumoniae* strain lacking the
350 *ccn* genes (Fig. S4C and F). While the *ccnABCDE* deletion did not cause *S. pneumoniae* to
351 express the capsule biosynthetic genes at a higher level (Tables S3 S4, and S5), we did observe
352 increased expression of genes in the Leloir pathway (*galK* and *galT2*), which is involved in the
353 synthesis of a precursor for capsular polysaccharide synthesis (UDP-glucose), in the Δ*ccnABCDE*
354 mutant as compare to its isogenic *ccn*$^+$ parental D39 strain when grown in BHI broth
355 supplemented with 0.2 mM $ZnSO_4$ (Table S5 and Fig. 8). Notably, increased production of
356 capsular polysaccharide precursors has been shown to increase capsule production (*33, 34*). In
357 future studies, we plan on rigorously testing this model that the Ccn sRNAs decrease capsule
358 synthesis by reducing expression of genes involved in synthesizing capsular polysaccharide

359 precursors leading to an increase in Mn uptake (Fig. 8). Moreover, we intend to evaluate the
360 molecular mechanism by which the Ccn sRNAs regulate expression of these genes.
361
362 **MATERIALS AND METHODS**
363 **Bacterial strains and growth conditions.** Bacterial strains used in this study were derived
364 from encapsulated *S. pneumoniae* serotype 2 strain D39W (*14*) and TIGR4 and are listed in Table
365 S1. Strains were grown on plates containing trypticase soy agar II (modified; Becton-Dickinson
366 [BD]) and 5% (vol/vol) defribrinated sheep blood (TSAII BA) at 37°C in an atmosphere of 5% CO_2,
367 and liquid cultures were statically grown in BD brain heart infusion (BHI) broth at 37°C in an
368 atmosphere of 5% CO_2. Bacteria were inoculated into BHI broth from frozen cultures or single,
369 isolated colonies. For overnight cultures, strains were first inoculated into a 17-mm-diameter
370 polystyrene plastic tube containing 5 mL of BHI broth and then serially diluted by 100-fold into
371 four tubes; these cultures were then grown for 10 to 16 h. Cultures with an optical density at 620
372 nm (OD_{620}) of 0.1 to 0.4 were diluted to a starting OD_{620} between 0.002 and 0.005 in 5 mL of BHI
373 broth in 16-mm glass tubes. Growth was monitored by measuring OD_{620} using a Genesys 30
374 visible spectrophotometer (ThermoFisher Scientific). For antibiotic selections, TSAII BA plates
375 and BHI cultures were supplemented with 250 µg kanamycin per mL, 150 µg streptomycin per
376 mL, or 0.3 µg erythromycin per mL.
377
378 **Construction and confirmation of mutants.** Mutant strains were constructed by
379 transformation of competent *S. pneumoniae* D39 and TIGR4 derived strains with linear PCR
380 amplicons as described previously (*35, 36*). DNA amplicons containing antibiotic resistance
381 markers were synthesized by overlapping fusion PCR using the primers listed in Table S2.
382 Competence was induced in *S. pneumoniae* D39 or TIGR4 derived cells with CSP-1 or CSP-2,
383 respectively, synthetic competence stimulatory peptide. Unmarked deletions of the target genes
384 were constructed using the *kan*^{R}-*rpsL*$^+$ (Janus cassette) allele replacement method as described

previously (*37*). In the first step, the Janus cassette containing *rpsL*$^{+}$ allele and a kanamycin resistance gene was used to disrupt target genes in an *rpsL1* or *rpsLK56T* (Str^{R}) strain background, and transformants were selected for kanamycin resistance and screened for streptomycin sensitivity. In the second step, the Janus cassette was eliminated by replacement with a PCR amplicon lacking antibiotic markers and the resulting transformants were selected for streptomycin resistance and screened for kanamycin sensitivity. Freezer stocks were made of each strain from single colonies isolated twice on TSAII BA plates containing antibiotics listed in Table S1. All strains were validated by PCR amplification and sequencing.

RNA extraction. To isolate RNA, strains were grown in 30 mL of BHI starting at an OD_{620} = 0.002 in 50 mL conical tubes. RNA was extracted from exponentially growing cultures of IU1781 (D39), NRD10220 (TIGR4), and their derived isogenic mutants lacking all five *ccn* genes, NRD10176 (D39 Δccn) and NRD10266 (TIGR4 Δccn), at $OD_{620} \approx 0.2$ using the FastRNA Pro Blue Kit (MP Bio) according to the manufacturer's guidelines. Briefly, cells were collected by centrifugation at 16,000 x g for 8 min at 4°C. Cell pellets were resuspended in 1 mL of RNApro™ solution (MP Bio) and processed five-times for 40 sec at 400 rpm in a BeadBug™ homogenizer (Benchmark Scientific). Cell debris was removed by centrifugation at 16,000 x g for 5 min at 4°C. After mixing 300 μL of chloroform with the supernatant, the aqueous and organic layers were separated by centrifugation at 16,000 x g for 5 min at 4°C. RNA was precipitated with 500 μL of ethanol at -80°C overnight. After collecting the precipitated RNA by centrifugation at 16,000 x g for 15 min at 4°C, the pellet was washed once with 75% ethanol and suspend in DEPC-treated water. The amount and purity of all RNA samples isolated were assessed by NanoDrop spectroscopy (Thermo Fisher).

Library preparation and mRNA-seq. cDNA libraries were prepared from total RNA Azenta Life Sciences. Briefly, total RNA was subjected to rRNA-depletion using the FastSelect 5S/16S/23S rRNA depletion kit for bacteria. Libraries were the generated with NEBNext Ultra™ II Directional RNA Library Prep Kit. 150 bp paired-end read sequencing was performed using an Illumina HiSeq4000 sequencer.

RNA-seq analysis. The raw sequencing reads were quality and adapter trimmed using Cutadapt version 4.1 with a minimum length of 18 nucleotides. The trimmed reads were then mapped on the *Streptococcus pneumoniae* D39 (Genbank CP000410) genome using Bowtie2 (*38*). HTseq version 2.0.2 was used to generate read counts for the genes (*39*). Differential gene expression was identified using the program DESeq2 with default parameters (*40*). Primary data from the mRNA-seq analyses were submitted to the NCBI Gene Expression Omnibus (GEO) and have the accession number GSE246655.

Reverse transcriptase-droplet digital PCR (RT-ddPCR) analysis. RT-ddPCR was performed as described previously (*41*). Isolated RNA was treated with DNase (TurboDNase, Ambion) as per manufacturer's instructions. Next, RNA (1 μg) was reverse transcribed using Superscript III reverse transcriptase (Invitrogen) with random hexamers. RT and No RT control (NRT) sample were utilized. These samples were diluted 1:10^1, 1:10^2, 1:10^3, or 1:10^6. Then, 2 µL of each diluted RT and NRT sample was added to a 22 µL reaction mixture containing 11 µL of QX200™ ddPCR ™ Evagreen Supermix (Bio-Rad) and 1.1 µL of each 2 µM ddPCR primers (Table S6). A single no template control (NTC) was included for each ddPCR primer pair used. Reactions were performed using at least three independent biological replicates. Droplets were generated using the QX200 Automated Droplet Generator (Bio-Rad), and end-point PCR was carried out using a C1000 Touch™ thermal cycler (Bio-Rad) following the manufacturer's instructions. Quantification

of PCR-positive and PCR-negative droplets in each reaction, which provides absolute quantification of the target transcript, was performed using the QX200 Droplet Reader (Bio-Rad). This data was analyzed with QuantaSoft software (Bio-Rad) to determine the concentration of each target expressed as copies per µL. Transcript copies were normalized to *tuf* mRNA (internal control) and fold changes of transcripts corresponding to target genes in different mutants relative to the WT parent were calculated. Statistical analysis was performed using Student's t-test with GraphPad Prism version 10.0.0.

Northern blot analysis. Northern blotting was conducted as previously described (*13*). Briefly, 3 µg of isolated RNA was fractionated on 10% polyacrylamide gels containing 7% urea by electrophoresis at 55 V and subsequently, transferred to a Zeta-probe membrane (Bio-Rad) using a Trans-Blot SD semidry transfer apparatus (Bio-rad) at 4 mA per cm^2 with a maximum of 400 mA for 50 min. RNA was then UV-crosslinked to the membrane with a Spectroline UV crosslinker with the "optimal crosslink" setting. 5'-Biotinylated probes were hybridized to the membrane overnight at 42°C in ULTRAhyb (Ambion) hybridization buffer. Blots were developed according to the BrightStar BioDetect kit protocol (Ambion), imaged with the ChemiDoc MP imager (Bio-Rad), and individual band intensities were quantified using Image Lab software version 5.2.1 (Bio-Rad). Signal intensities for each transcript were normalized to that of 5S rRNA, which served as a loading control. Graphs of normalized abundance of each transcript for three biological replicates were produced using GraphPad Prism version 10.0.0.

Inductively coupled plasma-mass spectrometry (ICP-MS) analysis. ICP-MS sample preparation was based on a previous publication (*42*), with some modifications. Bacteria were grown in BHI broth at 37°C with 5% CO_2 to OD_{620} = 0.2. Five mL of culture was centrifuged for 10 min in pre-chilled tubes at 12,400 x *g* at 4°C, and cell pellets were resuspended in 1.0 mL of

chilled BHI supplemented with 1 mM nitrilotriacetic acid (Sigma-Aldrich) (pH 7.2). Samples were centrifuged for 7 min at 16,100 x *g* at 4°C, and supernatants were removed. Pellets were centrifuged for an additional 3 min in the same way, and residual supernatant was removed. Cell pellets were washed twice with centrifugation in the same way with 1.0 mL of chilled 10X PBS (1.3M NaCl, 88mM Na_2HPO_4, 12mM NaH_2PO_4, pH 7.0) that had been treated with chelator. Similar ICP-MS results were obtained when cells were washed with 1X PBS instead of 10X PBS. Chelated PBS was prepared by mixing with 1% (wt/vol) Chelex-100 (BioRad), which was rotated overnight at 4°C and passed through a 0.22 µm Steriflip (MilliporeSigma) filter. Before the last centrifugation in PBS, samples were split into two 0.475 mL aliquots for ICP-MS analysis and protein quantification. After removal of supernatants, pellets for ICP-MS were dried for 15 h at low heat in an evaporative centrifuge and stored at -80°C until being processed for ICP-MS analysis. Pellets for protein determination were suspended in in 100 µL of lysis buffer (1% (wt/vol) SDS [Sigma], 0.1% w/v Triton X-100 [Mallinckrodt]) and stored at -80°C. Protein amount was determined by using the DC protein assay (BioRad). For ICP-MS analysis, dried samples were resuspended in 400 µL of 30% trace metal grade HNO_3 (Sigma). Samples and a 30% HNO_3 blank were heated at 95° C for 10 min with shaking at 500 rpm. Samples were then diluted 100-fold to a final volume of 3.0 mL with 2.5% HNO_3 containing the Pure Plus Internal Standard Mix (100 ppb, PerkinElmer). Samples were analyzed using an Agilent 8800 QQQ ICP-MS operating with hydrogen (^{55}Mn detection) or helium (^{66}Zn detection) as collision gases to remove possible interferences. ^{45}Sc or ^{72}Ge were used as internal references. Zn^{2+} and Mn^{2+} amounts were calculated from standard curves made with Pure Plus Multi-Element Calibration Standard 3 (0.5-100ppb, PerkinElmer). Metals amounts detected in the 30% HNO_3 blank were subtracted from all samples. Metal amounts in samples were normalized relative to total protein amounts in the matched samples.

Mouse models of infection: All procedures were approved in advance by UTHealth Animal Welfare Committee and carried out as previously described (*41*). Male ICR mice (21-24 g; Envigo) were anaesthetized by inhaling 4 to 5 % isoflurane. A total of 8 mice were intranasally inoculated with 10^7 CFU of a specific *S. pneumoniae* strain suspended in 50 μL of 1 X PBS prepared from cultures grown in BHI broth at 37°C in an atmosphere of 5% CO_2 to $OD_{620} \approx 0.1$. Mice were monitored visually at 4 to 8 h intervals, and isoflurane-anesthetized moribund mice were euthanized by cardiac puncture-induced exsanguination followed by cervical dislocation. Kaplan-Meir survival curves and log-rank tests were generated using GraphPad Prism 10.0.0 software.

SUPPLEMENTAL MATERIALS

Supplemental Materials are available for this article.

ACKNOWLEDGEMENTS

This work was supported by NIGMS grant T32GM131994 (to M.O.), NIGMS grant R35GM118157 (to D.P.G.), NIGMS grant R35GM131767 (to M.E.W.), McGovern Medical Startup funds, and NIAID grant R21AI171771 (to N.R.D.).

REFERENCES

1. D. G. Mediati, S. Wu, W. Wu, J. J. Tree, Networks of Resistance: Small RNA Control of Antibiotic Resistance. *Trends Genet* **37**, 35-45 (2021).
2. R. Ghandour, K. Papenfort, Small regulatory RNAs in *Vibrio cholerae*. *Microlife* **4**, uqad030 (2023).
3. K. Papenfort, S. Melamed, Small RNAs, Large Networks: Posttranscriptional Regulons in Gram-Negative Bacteria. *Annual Review of Microbiology*, (2023).
4. J. Hor, G. Matera, J. Vogel, S. Gottesman, G. Storz, Trans-Acting Small RNAs and Their Effects on Gene Expression in *Escherichia coli* and *Salmonella enterica*. *EcoSal Plus* **9**, (2020).
5. C. Pourciau, Y. J. Lai, M. Gorelik, P. Babitzke, T. Romeo, Diverse Mechanisms and Circuitry for Global Regulation by the RNA-Binding Protein CsrA. *Frontiers in Microbiology* **11**, 601352 (2020).
6. M. G. Jorgensen, J. S. Pettersen, B. H. Kallipolitis, sRNA-mediated control in bacteria: An increasing diversity of regulatory mechanisms. *Biochim Biophys Acta Gene Regul Mech* **1863**, 194504 (2020).

7. L. Bossi, N. Figueroa-Bossi, P. Bouloc, M. Boudvillain, Regulatory interplay between small RNAs and transcription termination factor Rho. *Biochim Biophys Acta Gene Regul Mech* **1863**, 194546 (2020).
8. F. Ponath, J. Hor, J. Vogel, An overview of gene regulation in bacteria by small RNAs derived from mRNA 3' ends. *FEMS Microbiology Reviews* **46**, (2022).
9. G. B. D. L. R. I. Collaborators, Estimates of the global, regional, and national morbidity, mortality, and aetiologies of lower respiratory infections in 195 countries, 1990-2016: a systematic analysis for the Global Burden of Disease Study 2016. *Lancet Infect Dis* **18**, 1191-1210 (2018).
10. P. Acebo, A. J. Martin-Galiano, S. Navarro, A. Zaballos, M. Amblar, Identification of 88 regulatory small RNAs in the TIGR4 strain of the human pathogen *Streptococcus pneumoniae*. *RNA* **18**, 530-546 (2012).
11. R. Kumar *et al.*, Identification of novel non-coding small RNAs from *Streptococcus pneumoniae* TIGR4 using high-resolution genome tiling arrays. *BMC Genomics* **11**, 350 (2010).
12. B. Mann *et al.*, Control of virulence by small RNAs in *Streptococcus pneumoniae*. *PLoS Pathogens* **8**, e1002788 (2012).
13. D. Sinha *et al.*, Redefining the sRNA Transcriptome in *Streptococcus pneumoniae* Serotype 2 Strain D39. *Journal of Bacteriology*, (2019).
14. J. Slager, R. Aprianto, J. W. Veening, Deep genome annotation of the opportunistic human pathogen *Streptococcus pneumoniae* D39. *Nucleic Acids Research* **46**, 9971-9989 (2018).
15. H. C. Tsui *et al.*, Identification and characterization of noncoding small RNAs in *Streptococcus pneumoniae* serotype 2 strain D39. *Journal of Bacteriology* **192**, 264-279 (2010).
16. A. Halfmann, M. Kovacs, R. Hakenbeck, R. Bruckner, Identification of the genes directly controlled by the response regulator CiaR in *Streptococcus pneumoniae*: five out of 15 promoters drive expression of small non-coding RNAs. *Molecular Microbiology* **66**, 110-126 (2007).
17. K. Hentrich *et al.*, *Streptococcus pneumoniae* Senses a Human-like Sialic Acid Profile via the Response Regulator CiaR. *Cell Host Microbe* **20**, 307-317 (2016).
18. P. D. Rogers *et al.*, Gene expression profiling of the response of *Streptococcus pneumoniae* to penicillin. *J Antimicrob Chemother* **59**, 616-626 (2007).
19. A. Schnorpfeil *et al.*, Target evaluation of the non-coding csRNAs reveals a link of the two-component regulatory system CiaRH to competence control in *Streptococcus pneumoniae* R6. *Molecular Microbiology* **89**, 334-349 (2013).
20. F. E. Jacobsen, K. M. Kazmierczak, J. P. Lisher, M. E. Winkler, D. P. Giedroc, Interplay between manganese and zinc homeostasis in the human pathogen *Streptococcus pneumoniae*. *Metallomics* **3**, 38-41 (2011).
21. J. E. Martin, J. P. Lisher, M. E. Winkler, D. P. Giedroc, Perturbation of manganese metabolism disrupts cell division in *Streptococcus pneumoniae*. *Molecular Microbiology* **104**, 334-348 (2017).
22. B. A. Eijkelkamp *et al.*, Extracellular zinc competitively inhibits manganese uptake and compromises oxidative stress management in *Streptococcus pneumoniae*. *PloS One* **9**, e89427 (2014).
23. A. L. McFarland, N. Bhattarai, M. Joseph, M. E. Winkler, J. E. Martin, Cellular Mn/Zn Ratio Influences Phosphoglucomutase Activity and Capsule Production in *Streptococcus pneumoniae* D39. *Journal of Bacteriology* **203**, e0060220 (2021).
24. C. A. McDevitt *et al.*, A molecular mechanism for bacterial susceptibility to zinc. *PLoS pathogens* **7**, e1002357 (2011).

25. J. E. Martin *et al.*, The zinc efflux activator SczA protects *Streptococcus pneumoniae* serotype 2 D39 from intracellular zinc toxicity. *Molecular Microbiology* **104**, 636-651 (2017).
26. A. D. Ogunniyi *et al.*, Central role of manganese in regulation of stress responses, physiology, and metabolism in *Streptococcus pneumoniae*. *Journal of Bacteriology* **192**, 4489-4497 (2010).
27. J. W. Rosch, G. Gao, G. Ridout, Y. D. Wang, E. I. Tuomanen, Role of the manganese efflux system *mntE* for signalling and pathogenesis in *Streptococcus pneumoniae*. *Molecular Microbiology* **72**, 12-25 (2009).
28. J. E. Martin *et al.*, A Mn-sensing riboswitch activates expression of a Mn^{2+}/Ca^{2+} ATPase transporter in Streptococcus. *Nucleic Acids Research* **47**, 6885-6899 (2019).
29. A. Dintilhac, G. Alloing, C. Granadel, J. P. Claverys, Competence and virulence of *Streptococcus pneumoniae*: Adc and PsaA mutants exhibit a requirement for Zn and Mn resulting from inactivation of putative ABC metal permeases. *Molecular Microbiology* **25**, 727-739 (1997).
30. R. Novak, J. S. Braun, E. Charpentier, E. Tuomanen, Penicillin tolerance genes of *Streptococcus pneumoniae*: the ABC-type manganese permease complex Psa. *Molecular Microbiology* **29**, 1285-1296 (1998).
31. N. S. Jakubovics, A. W. Smith, H. F. Jenkinson, Expression of the virulence-related Sca (Mn^{2+}) permease in *Streptococcus gordonii* is regulated by a diphtheria toxin metallorepressor-like protein ScaR. *Molecular Microbiology* **38**, 140-153 (2000).
32. J. W. Johnston, D. E. Briles, L. E. Myers, S. K. Hollingshead, Mn^{2+}-dependent regulation of multiple genes in *Streptococcus pneumoniae* through PsaR and the resultant impact on virulence. *Infection and Immunity* **74**, 1171-1180 (2006).
33. C. L. Ventura, R. T. Cartee, W. T. Forsee, J. Yother, Control of capsular polysaccharide chain length by UDP-sugar substrate concentrations in *Streptococcus pneumoniae*. *Molecular Microbiology* **61**, 723-733 (2006).
34. M. B. Ayoola *et al.*, Polyamine Synthesis Effects Capsule Expression by Reduction of Precursors in *Streptococcus pneumoniae*. *Frontiers in Microbiology* **10**, 1996 (2019).
35. S. Ramos-Montanez *et al.*, Polymorphism and regulation of the *spxB* (pyruvate oxidase) virulence factor gene by a CBS-HotDog domain protein (SpxR) in serotype 2 *Streptococcus pneumoniae*. *Molecular Microbiology* **67**, 729-746 (2008).
36. K. E. Bruce, B. E. Rued, H. T. Tsui, M. E. Winkler, The Opp (AmiACDEF) Oligopeptide Transporter Mediates Resistance of Serotype 2 *Streptococcus pneumoniae* D39 to Killing by Chemokine CXCL10 and Other Antimicrobial Peptides. *Journal of Bacteriology* **200**, (2018).
37. K. M. Kazmierczak, K. J. Wayne, A. Rechtsteiner, M. E. Winkler, Roles of rel_{Spn} in stringent response, global regulation and virulence of serotype 2 *Streptococcus pneumoniae* D39. *Molecular Microbiology* **72**, 590-611 (2009).
38. B. Langmead, S. L. Salzberg, Fast gapped-read alignment with Bowtie 2. *Nature Methods* **9**, 357-359 (2012).
39. S. Anders, P. T. Pyl, W. Huber, HTSeq--a Python framework to work with high-throughput sequencing data. *Bioinformatics* **31**, 166-169 (2015).
40. M. I. Love, W. Huber, S. Anders, Moderated estimation of fold change and dispersion for RNA-seq data with DESeq2. *Genome Biol* **15**, 550 (2014).
41. D. Sinha, J. P. Frick, K. Clemons, M. E. Winkler, N. R. De Lay, Pivotal Roles for Ribonucleases in *Streptococcus pneumoniae* Pathogenesis. *mBio*, e0238521 (2021).
42. Y. Fu *et al.*, A new structural paradigm in copper resistance in *Streptococcus pneumoniae*. *Nat Chem Biol* **9**, 177-183 (2013).

619 **FIGURES**

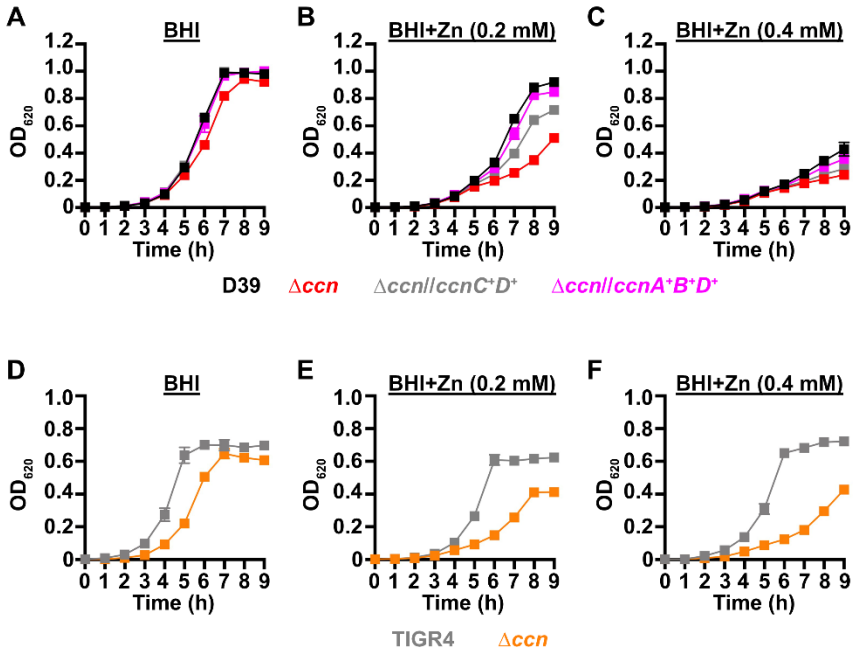

620

621 **Figure 1:** Growth phenotypes of *S. pneumoniae* strains harboring deletion of the *ccn* genes.
622 Growth characteristics at 37°C under an atmosphere of 5% CO_2 in BHI broth alone (A, D) or with
623 0.2 mM (B, E) or 0.4 mM (C,F) $ZnSO_4$ of following strains: (A, B, C) IU781 (D39), NRD10176
624 (Δ*ccn*), NRD10396 (Δ*ccnI*//*ccnA*$^+$*B*$^+$*D*$^+$), and NRD10397 (Δ*ccnI*//*ccnC*$^+$*D*$^+$); (D, E, F) NRD10220
625 (TIGR4) and NRD10266 (Δ*ccn*). Each point on the graph represents the mean OD_{620} value from
626 three independent cultures. Error bars, which in some cases are too small to observe in the graph,
627 represent the standard deviation (SD).

628

629

630

631

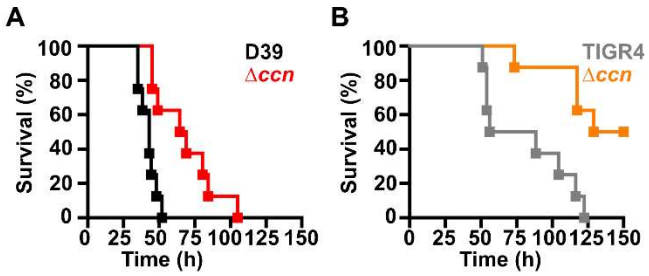

Figure 2: Virulence phenotypes of *S. pneumoniae* strains harboring deletion of the *ccn* genes. Survival curve of ICR outbred mice after infection with ~10^7 CFU in a 50 μL inoculum of the following *S. pneumoniae* strains: (A) IU1781 (D39) and NRD10176 (Δ*ccn*); (C) NRD10220 (TIGR4) and NRD10266 (Δ*ccn*). Eight mice were infected per strain. Disease progression of animals was monitored, the time at which animals reached a moribund state was recorded, and these mice were subsequently euthanized as described in Materials and Methods. A survival curve was generated from this data and analyzed by Kaplan-Meier statistics and log rank test to determine P-values.

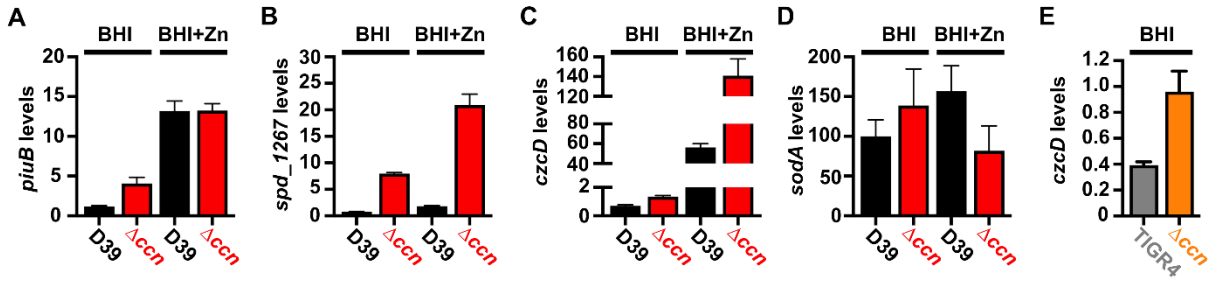

Figure 3: Loss of the *ccn* genes perturbs the expression of Zn and Mn stress associated genes in *S. pneumoniae*. Abundance of *piuB* (A), *spd_1267* (B), *czcD* (C, E), and *sodA* (D) mRNAs was determined by RT-ddPCR (A, B, and C) or northern blot analyses (D) as described in Materials and Methods for strain IU1781 (D39) and derived Δ*ccnABCDE* mutant strain (NRD10176; Δ*ccn*) grown to exponential phase (OD_{620} of ~0.2) in BHI broth alone (BHI) or supplemented with 0.2

649 mM Zn (BHI+Zn) at 37°C under an atmosphere of 5% CO_2. (E) Expression of *czcD* was
650 determined by RT-ddPCR analyses for NRD10220 (TIGR4) and derived Δ*ccnABCDE* mutant
651 strain NRD10266 (Δ*ccn*) grown to exponential phase in BHI Broth at 37°C under an atmosphere
652 of 5% CO_2. Transcript levels were normalized to *tuf* (A, B, C, and E) or 5S rRNA (D). Values
653 represent the mean of three independent cultures and error bars indicate SEM.
654
655

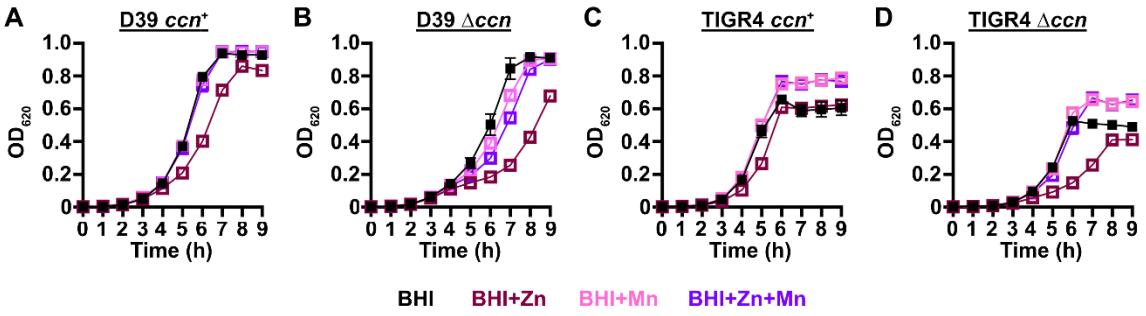

656

657 **Figure 4:** Mn supplementation eliminates the Zn dependent growth inhibition of *S. pneumoniae*
658 Δ*ccnABCDE* mutant. Growth characteristics at 37°C under an atmosphere of 5% CO_2 in BHI broth
659 alone (BHI) or with 0.2 mM $ZnSO_4$ (BHI+Zn), 0.2 mM $MnCl_2$ (BHI+Mn), or 0.2 mM $ZnSO_4$ and
660 $MnCl_2$ (BHI+Zn+Mn) of strains (A) IU1781 (D39 *ccn*$^+$), (B) NRD10176 (D39 Δ*ccn*), (C), NRD10220
661 (TIGR4 *ccn*$^+$), and (D) NRD10266 (TIGR4 Δ*ccn*). Each point on the graph represents the mean
662 OD_{620} value from three independent cultures. Error bars, which in some cases are too small to
663 observe in the graph, represent the standard deviation (SD).
664
665
666
667
668
669

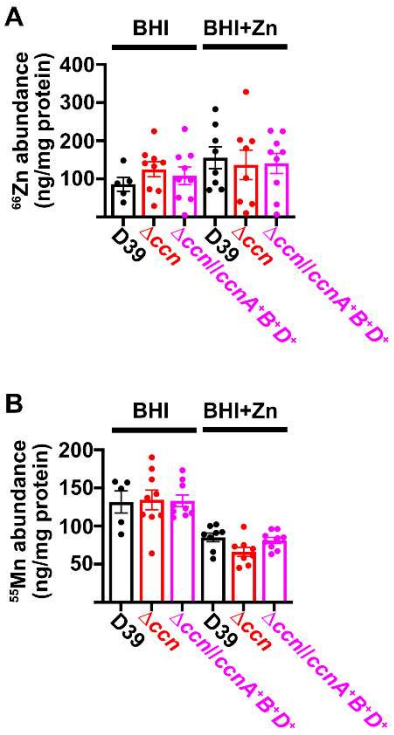

Figure 5: Deletion of the *ccn* genes reduces total cell associated Mn, but not Zn levels. Total cell associated Zn (A) and Mn (B) was measured from cells harvested from cultures of IU781 (D39), NRD10176 (Δ*ccn*), and NRD10396 (Δ*ccn//ccnA*$^+$*B*$^+$*D*$^+$) grown to exponential growth phase (OD_{620} of ~0.2) in BHI broth alone (BHI) or with 0.2 mM ZnS04 (BHI+Zn) by ICP-MS and normalized to protein amounts. Results represent the mean of 5 to 9 replicates with values from each replicate shown as a point. Error bars indicate SEM.

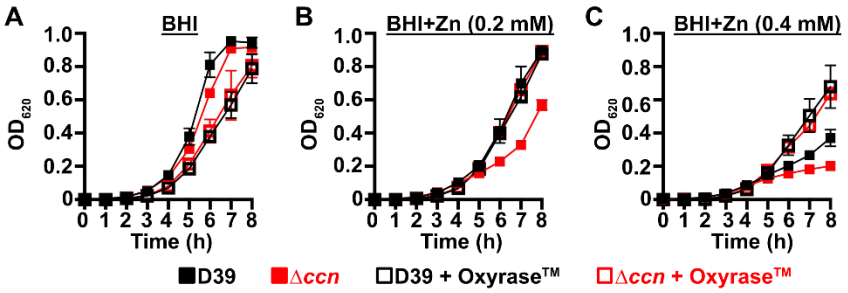

Figure 6: Depletion of O_2 abolishes the Zn hypersensitivity of the *S. pneumoniae* Δ*ccnABCDE* mutant. Growth characteristics at 37°C under an atmosphere of 5% CO_2 in BHI broth alone (A) or with 0.2 mM (B) or 0.4 mM (C) $ZnSO_4$ of IU781 (D39) and NRD10176 (Δ*ccn*) in the absence or presence of 10% (volume/volume) Oxyrase™. Each point on the graph represents the mean OD_{620} value from three independent cultures. Error bars, which in some cases are too small to observe in the graph, represent the standard deviation (SD).

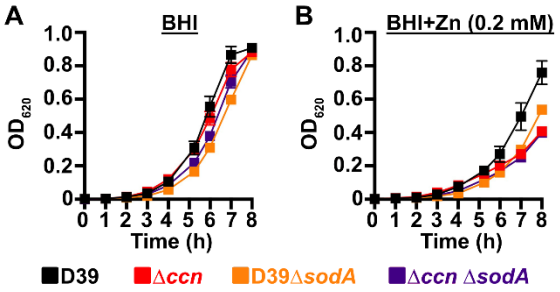

Figure 7: A *S. pneumoniae* Δ*sodA* mutant phenocopies the Zn hypersensitivity of a Δ*ccnABCDE* mutant strain. Growth characteristics at 37°C under an atmosphere of 5% CO_2 in BHI broth alone (A) or with 0.2 mM $ZnSO_4$ (B) of IU781 (D39), NRD10176 (Δ*ccn*), NRD10533 (D39 Δ*sodA*), and NRD10534 (Δ*ccn* Δ*sodA*). Each point on the graph represents the mean OD_{620} value from three independent cultures. Error bars, which in some cases are too small to observe in the graph, represent the standard deviation (SD).

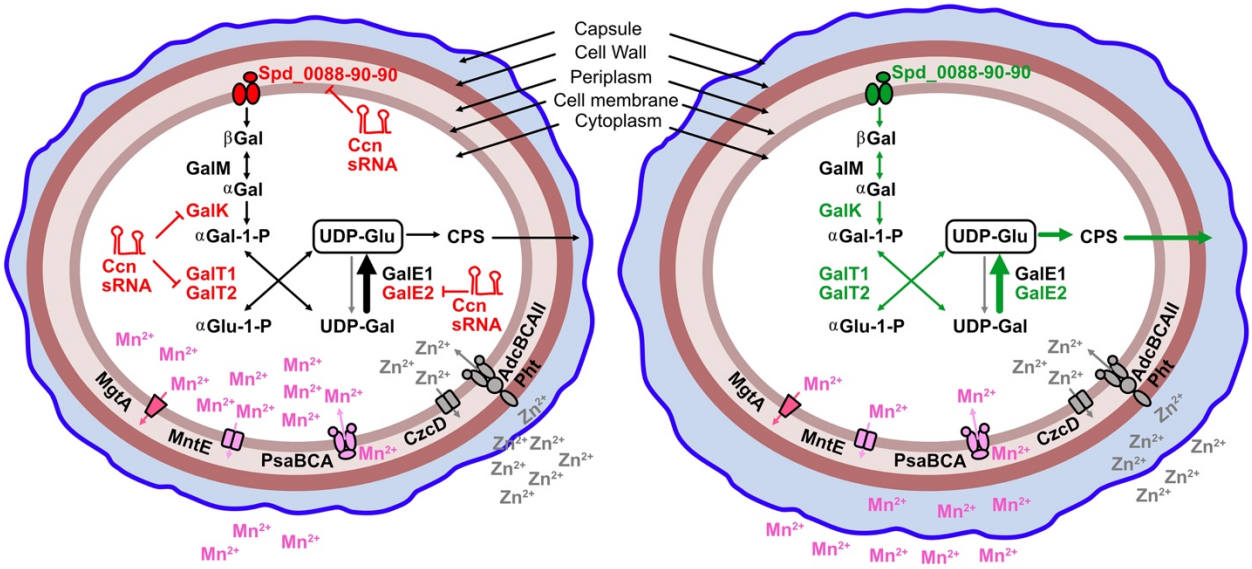

Figure 8: Model of the function of the Ccn sRNAs in regulating Mn homeostasis. The Ccn sRNAs down-regulate expression of Leloir pathway (*galK*, *galT2*, *galT1*, *galE2*) and galactose transport genes (*spd_0088*, *spd_0089*, *spd_0090*) resulting in reduced CPS synthesis and thus, a thinner capsule, which improves Mn uptake (pneumococcal cell on the left). In the absence of the Ccn sRNAs, increased expression of the Leloir pathway genes leads to increased production of capsule precursors and consequently, increased capsule thickness limiting Mn uptake (pneumococcal cell on the right). MgtA (Ca^{2+}/Mn^{2+} exporter); MntE (primary Mn^{2+} exporter); PsaBCA (only known Mn^{2+} importer); CzcD (Cd^{2+}/Zn^{2+} exporter); Pht (histidine triad proteins that bind Zn^{2+} and transfer to AdcAII); AdcBCAII (Zn^{2+} import system).